An interpretation of SPring-8 ground elevation by the empirical ATL-law approach

Y. Okayasu,[a,1] **S. Matsui,**[b] **C. Zhang**[a] **and H. Kimura**[c]

[a]*Japan Synchrotron Radiation Research Institute,*
 1-1-1, Kouto, Sayo-cho, Sayo-gun, Hyogo 679-5198, Japan

[b]*RIKEN SPring-8 Center,*
 1-1-1, Kouto, Sayo-cho, Sayo-gun, Hyogo 679-5198, Japan

[c]*National Institute for Quantum and Radiological Science and Technology,*
 Kansai Photon Science Institute, Harima District 1-1-1, Kouto,
 Sayo-cho, Sayo-gun, Hyogo 679-5148, Japan

 E-mail: okayasu@spring8.or.jp

ABSTRACT: Starting in 1996, the coordinates of the accelerator components on the SPring-8 storage ring were continuously surveyed for over two decades. The dispersion of the elevation changes of the ground motion $\langle dz^2 \rangle$ analyzed from the aspect of the empirical ATL-law which has been intensively researched since 1990s. With the ATL-law, $\langle dz^2 \rangle$ can be expressed as products of a ground diffusion coefficient A, temporal survey spans T, and spatial scales L. The coefficient A is well known to depend on the local geology and is evaluated as $(7.6 \pm 1.4) \times 10^{-6}$ μm^2/s/m for the SPring-8 storage ring. In this paper, a transition of survey methods in the SPring-8 storage ring is reviewd and survey results both in horizontal and vertical directions are presented. Furthermore, the relevance of the ATL-law approach for the ground elevation dispersion are discussed.

---

[1]Corresponding author. Current affiliation: High Energy Accelerator Research Organization (KEK), Tsukuba, Japan.

Contents

1 Introduction

Many electron-synchrotron accelerator facilities are planning upgrades that might be called the fourth-generation synchrotron light sources. One common characteristic of the upgrades is to realize an ultra-low emittance by a diffraction limit in the X-ray region. To achieve this goal, various accelerator components, such as multi-pole magnets, beam monitors, and vacuum chambers must be precisely aligned with a sub-hundred μm (rms) order. Innovative alignment techniques have been developed and introduced for precise alignments, including a laser-based alignment system [1, 2] and a vibrating-wire magnet alignment method [3]. Furthermore, understanding ground motion trends for each facility is absolutely necessary to stabilize their performance prior to precise alignment. Therefore, storing and interpreting the continuous survey data over the long term are crucial. Particularly, in the 1990s a stochastic diffusive component of the elevation changes in the lower frequencies was found by Baklakov et al. [4] to obey an empirical ATL-law, which is associated with ground diffusive coefficient A, temporal survey span T, and geological scale L. Attempts to interpret the ground elevation changes with the ATL-law have been done by Shiltsev [5] at various accelerator facilities (except SPring-8). Recently, this ATL-law approach is expansively examined from the aspect of the fractal structure of the elevation changes by Suwada [10].

The SPring-8 (Super Photon ring 8 GeV) storage ring with a circumference of 1436 m, the world's largest third-generation synchrotron radiation facility (see figure 1, *upper*), is surrounded by Mt. Miharakuri (341 m above sea level). The ring consists 48 cell units (44 normal cells and 4 long-straight sections) with the Chasman-Green lattice configuration [6]. One normal cell consists of two bending magnets as well as multi-pole and correction magnets mounted on three common girders (figure 1, *lower*).
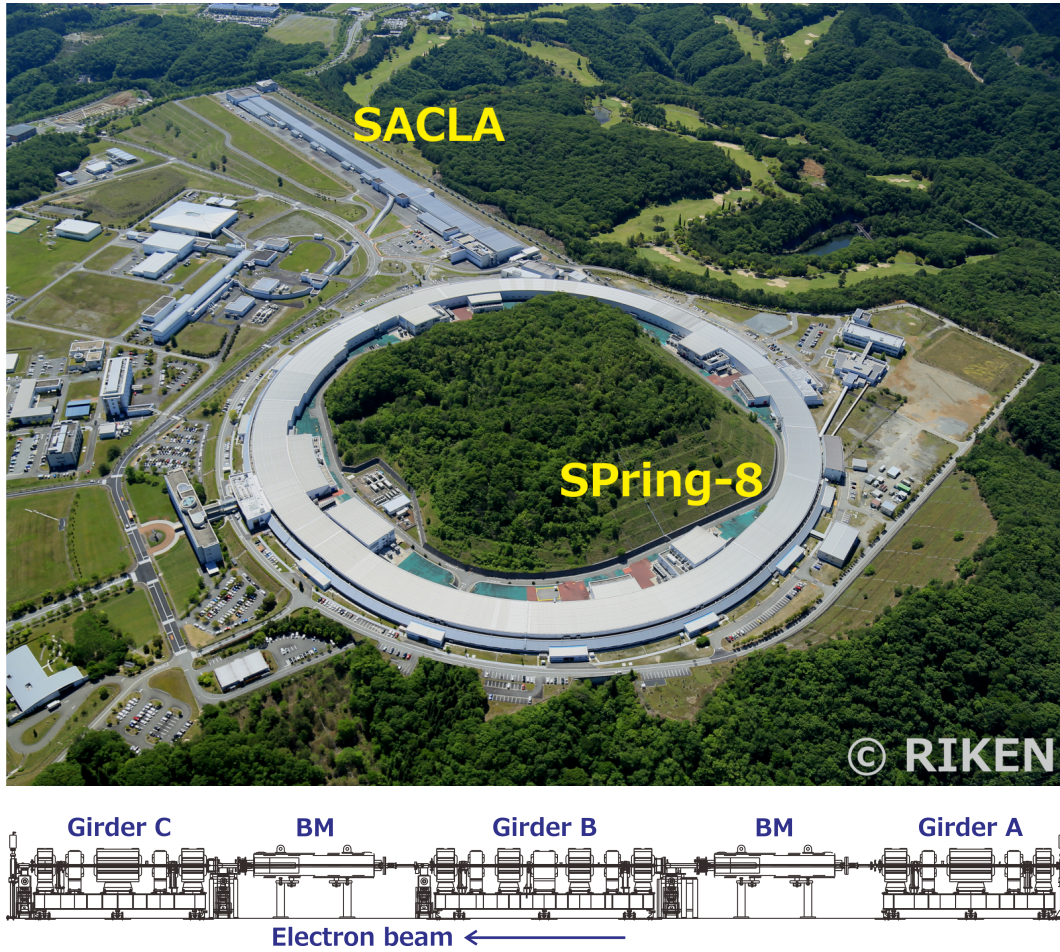
Figure 1. Bird's eye view of SPring-8/SACLA accelerator facilities (*upper*) and schematic side view of accelerator components for a normal one cell in storage ring tunnel (*lower*).

The coordinates of the quadrupole magnets on both ends of the common girders and the fiducial points on the accelerator tunnel wall for the entire ring were continuously surveyed for over two decades starting in 1996 (the beginning of services: 1997). The following are the survey's two goals: 1) understanding the trends of the coordinates changes of the accelerator components and 2) preparation to realign the accelerator components in case of such unexpected events as earthquakes or machine maintenance.

In this paper, we organize all of the measured data and focus on the level trends. We also interpret the ground elevation change, which is a major source of the magnets' level variation, and discuss applications of the *ATL*-law.

2 Survey details

For the SPring-8 storage ring survey, we have total 392 observation points. The details of the observation points are as follows: 264 quadrupole magnets (2 quadrupole magnets on both ends of 3 common girders for each normal cell), 24 monuments (6 monuments attached on insertion

devices for each long-straight section), and 104 monuments mounted on the accelerator tunnel wall (2 for each normal cell and 4 for each long-straight section). Our survey methods of the accelerator components in the storage ring tunnel can be roughly classified into the following three phases:

1) from the installation's beginning to a period when the configuration of the accelerator components were stabilized at long-straight sections: 1996–2003 (Phase I);

2) survey method was established: 2005–2013 (Phase II);

3) survey method was improved: 2014– (Phase III).
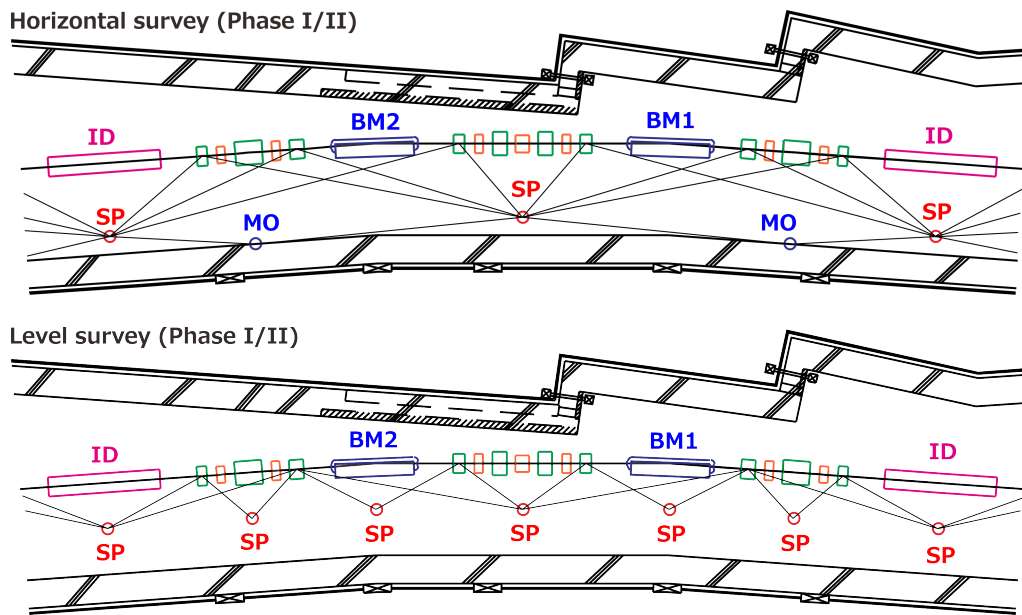
2.1 Phase I and II surveys

Figure 2. Schematics of network horizontal (*upper*) and level (*lower*) survey in SPring-8 storage ring (normal cell) during Phases I and II. SP, MO, ID, and BM represent station points, reference monuments mounted on accelerator tunnel wall, insertion devices, and bending magnets, respectively.

A schematic top view of the station points (SP) and the reference monuments (MO) mounted on the accelerator tunnel wall are described in figure 2 for both horizontal and level surveys. The insertion devises and the bending magnets are indicated as ID, BM1, and BM2. During the Phase I survey, a Leica SMART310 laser tracker and a Wild N3 precise level were utilized for the horizontal survey (up to ~25 m distance) and the level survey, respectively. Leica SMART310, the world's first three-dimensional mobile-tracking system, provides three-dimensional spherical coordinates of a target in space with nominal accuracy of a distance resolution of 1.26 μm and an angular resolution of 0.7 arcsection Since the laser tracker's accuracy is affected by its operating environment, the temperature, the pressure, the calibration, the condition of a spherically mounted retroreflector (SMR), and the operators, the actual accuracy of the Leica SMART310 was estimated with a laser interferometer system (Hewlett-Packard 5527A) in the storage ring. We eventually evaluated distance accuracy of 0.001 mm + 0.2 ppm and angular accuracy of ~10 μrad.

In 2000 a Zeiss DiNi11 digital level was introduced for a precise level survey to reduce human error. In the Phase II survey, a Leica Wild T3000 theodolite and a Kern ME5000 mekometer were complementarily introduced for precise-angle and long-distance measurements in addition to the laser tracker. Horizontal and vertical coordinates of all the measured magnets were independently analyzed and optimized by the least square method. Details for the first monument survey which was done in January 1993 before the accelerator construction, magnets installation, and its precise alignment procedure are described in [7].

2.2 Phase III survey

The Leica AT-402 laser tracker was introduced and replaced with the Leica SMART310 since its measurement distance significantly improved from 25 m to 160 m. As a result, the number of observation points per one station point was drastically increased as shown in figure 3 (*upper*) comparing to figure 2 (*upper*). On the other hand, we reduced the number of level survey points, which are located on quadrupole magnets and insertion devices, from 288 to 48 with the Trimble DiNi0.3 digital level (figure 3, *lower*). In this phase, only levels of most upstream quadrupole magnet mounted on the second girder (figure 1, *lower, "Girder B"*) in each normal cell (44 points) and monuments attached on insertion devices in each long-straight section (4 points) were measured in order to improve both survey work's efficiency and quality. All of the measured magnet coordinates were optimized by the least square method through the network analysis weighting 48 level data sets, which were complementarily measured by the digital level with higher accuracy comparing to the laser tracker, from the Phase III survey [8, 9]. As a result, mis-closure of the magnet levels along designed orbit was improved by 0.2 ∼ 0.3 mm for Phase III survey while 5 ∼ 6 mm for Phase I and II.
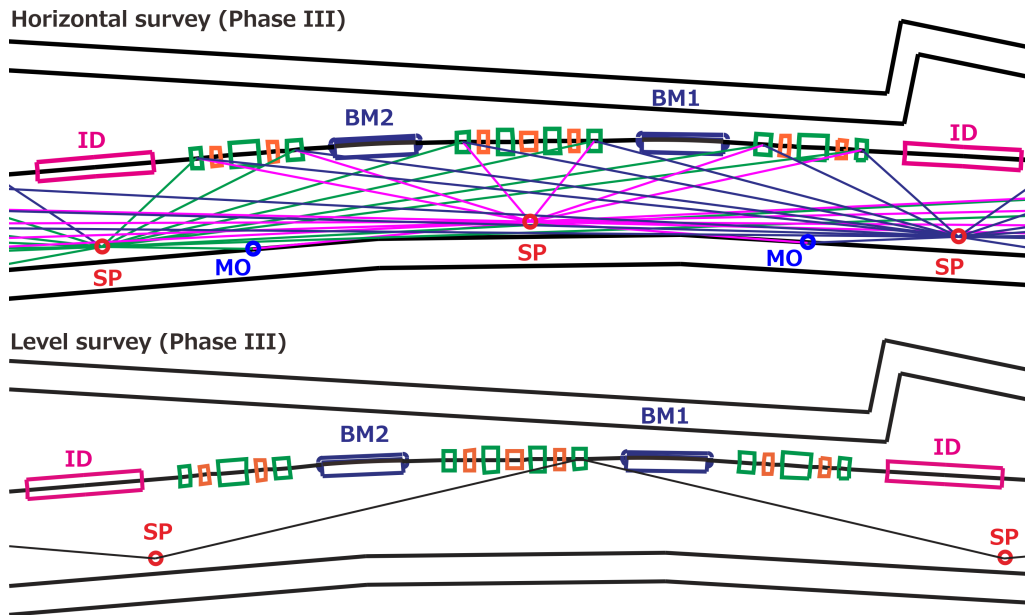

Figure 3. Schematics of network horizontal (*upper*) and level (*lower*) survey in SPring-8 storage ring (normal cell) during Phase III. SP, MO, ID, and BM represent station points, reference monuments mounted on accelerator tunnel wall, insertion devices, and bending magnets, respectively.

Table 1. Designed accuracies of instruments for SPring-8 storage ring survey.

Phase I/II	
Leica SMART310 (3D-coordinates)	
Angle (both horizontal and vertical)	±2.5 arcsec
Distance	< ±20 μm
Leica Wild N3 / Zeiss DiNi11	
Level	0.2 mm[†]
Leica Wild T3000	
Angle (both horizontal and vertical)	0.5 arcsec (nominal)
Kern ME5000	
Distance	200 μm + 0.2 ppm (nominal)
Phase III	
Leica AT-402 (3D-coordinates)	
Horizontal angle	0.6 ± 0.2 arcsec
Vertical angle	0.4 ± 0.1 arcsec
Distance	$6.5^{+2.3}_{-2.9}$ μm
Trimble DiNi0.3	
Level	0.3 mm[†]

[†]: this is the standard deviation for 1-km double-run leveling.

The designed accuracies of the typical instruments of the SPring-8 storage ring survey are summarized in table 1.

3 Survey results

The three-dimensional coordinates of the SPring-8 storage ring magnets were continuously surveyed from January 1996 to August 2018 by the above measurement schemes. This section compares and discusses dividing the horizontal and vertical components of both the seasonal and two decades of changes of the measured coordinates.

3.1 Horizontal variation

Horizontal coordinates can be separated into two components: radial and azimuth directions that define the origin at the center of the storage ring. First, we compared the seasonal changes for both the radial and azimuth directions along designed orbit distance D with three data sets measured on August 2018, February 2018, and August 2017 (figure 4).

In figure 4, the origins of both the radial and azimuth coordinates are oriented at $D = 0$ m, i.e., the coordinate of the most upstream magnet on the first cell 01 (C01). For the radial direction, the distribution of the amplitudes of two opposite seasonal changes is almost symmetric. Two prominent seasonal changes, −500 ∼ 500 μm and −440 ∼ 590 μm, are found at around $D = 560$ and 1340 m respectively, where a rainwater drain pipe and a beam transport tunnel are located 2 ∼ 3 m beneath the floor. The sum of the two seasonal changes varies within −210 ∼ 280 μm.
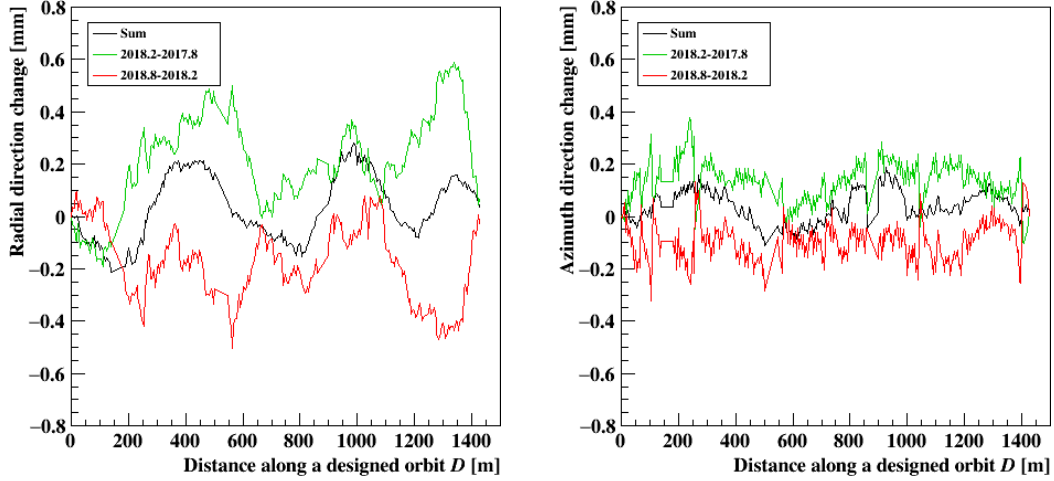
Figure 4. Seasonal coordinate changes in radial (*left*) and azimuth (*right*) directions of storage ring magnets. In both figures, *dash-dot-line* represents a direction change by subtracting February 2018 data from August 2018 data (hereafter referred as 2018.8–2018.2) and *dashed-lines* are 2018.2–2017.8. *Solid-lines* are their sum.
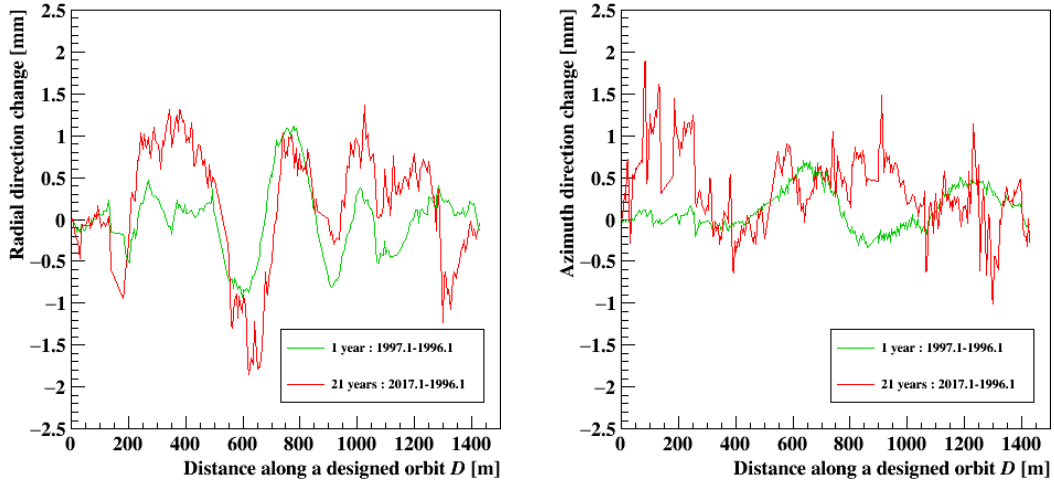

Figure 5. Comparisons of 1 year (1997.1–1996.1, *dashed-line*) and 21 years (2017.1–1996.1, *solid-line*) changes of radial (*left*) and azimuth (*right*) directions along the storage ring's designed orbit.

For the azimuth direction, the symmetric seasonal variations are limited to a comparison of the radial one, distributed around $D = 100$, 240, 560, and 1400 m, where an RF wave guide, an underpass, the rainwater drain pipe, and a transport tunnel also exist beneath the floor, respectively. The sum of the two seasonal changes are smaller than the radial one and varies from -110 to 190 μm.

As the sum distributions of both the radial and azimuth directions show, the two opposite seasonal changes do not completely cancel each other out. Their remaining components may vanish or accumulate gradually, and their behavior trends can be interpreted as systematic changes. Figure 5 compares the changes in both the radial (*left*) and azimuth (*right*) directions for two decades: 1 year (1997.1–1996.1, *dashed-line*) and 21 years (2017.1–1996.1, *solid-line*).

The azimuth direction changes for two decades (figure 5, *right, solid-line*) show quite an equivalent distribution, as the sum distribution in figure 4 (*right, solid-line*) compared to the radial directions. This means the trends of the azimuth direction changes (meaning both direction and gradient) along the storage ring are almost unique, and systematic changes are dominant, unlike in the radial direction. On the other hand, the amplitudes of the two decades of the radial direction changes around $D = 400$ and 1000 m, which correspond to the cutting and banking regions respectively, are almost equivalent, as shown by the sum distribution in figure 4 (*left, solid-line*).
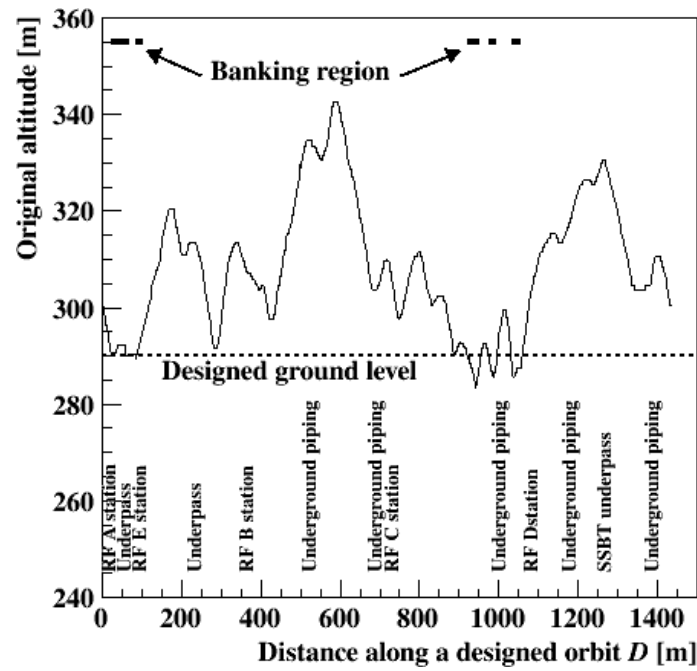
3.2 Vertical variation

Figure 6. Original altitude distribution along a designed orbit before SPring-8 storage ring construction. Designed ground level of 292 m is overlaid as a *dashed-line* and details of underground structures are also presented. Banking was carried out at around $D = 20 \sim 70$, $80 \sim 100$, $920 \sim 950$, $980 \sim 1000$, $1030 \sim 1060$ m, as marked with *bold-lines*.

First, to understand the vertical variation trends, the original altitude distribution along a designed orbit of the SPring-8 storage ring before its construction was presented with a designed ground level and the underground structures (figure 6). The banking regions are also overlaid with *bold-lines*. At least two trends can be recognized through the survey results: 1) banking areas and underground structures remain full, causing ground subsidence, 2) ground upheaval continues in the cut-up areas. The former trend was probably caused by the soil and concrete structures that have been compressed by the building load and the latter by the load's removal.

Seasonal elevation changes are compared in figure 7 (*left*) by subtracting the two data sets measured in opposite seasons: February and August. *Dashed* and *dash-dot-lines* represent elevation changes of 2018.8–2018.2 and 2018.2–2017.8, and their total is calculated and drawn as a *solid-line*. Equivalent to the seasonal changes of the radial direction (figure 4, *left*), the distributions of both

elevation changes are quite symmetric. Four major peaks of their sum distribution can be found at around $D = 100, 300, 500, 600$, and 1000 m. Underground structures exist, including an RF wave guide (~100 m), an underpass (~ 300 m), a ground cutting area (400 ~ 700 m) and a ground banking area (900 ~ 1000 m). The sum distribution deflects from $-340\,\mu$m to $180\,\mu$m.

We also compared the elevation changes for two decades with two data sets: 2017.1–1996.1 and 1997.1–1996.1 (figure 7, *right*). Prominent elevation and subsidence can be found at the ground cutting and banking areas, respectively.

Next we present the elevation trends of the storage ring magnets, which were continuously measured since January 1996 to August 2018, as contour plots and overlaid on the ground contour line and infrastructures on the SPring-8/SACLA accelerator complex (figure 8). The notations describe the underground structures and the ground constructions at locations of interest. 271 fiducial point level trends are plotted along the radial direction of the ring whose inner edge starts from January 1996 and whose outer edge ends by August 2018. We found that the measured level was apparently reflected by the underground structures and the topography before the construction. Over the past 20 years, the ground level has risen by as much as 2.5 mm at C14 to C24 (ground cutting area, which corresponds to $400 < D$ [m] < 700) or sunk as much as 1.5 mm at C31 to C36 (ground banking area, $900 < D$ [m] < 1000). At most sinking of 1 mm was found at the underground constructions that straddle the ring, such as rainwater drain pipes, RF waveguides, and underpasses.
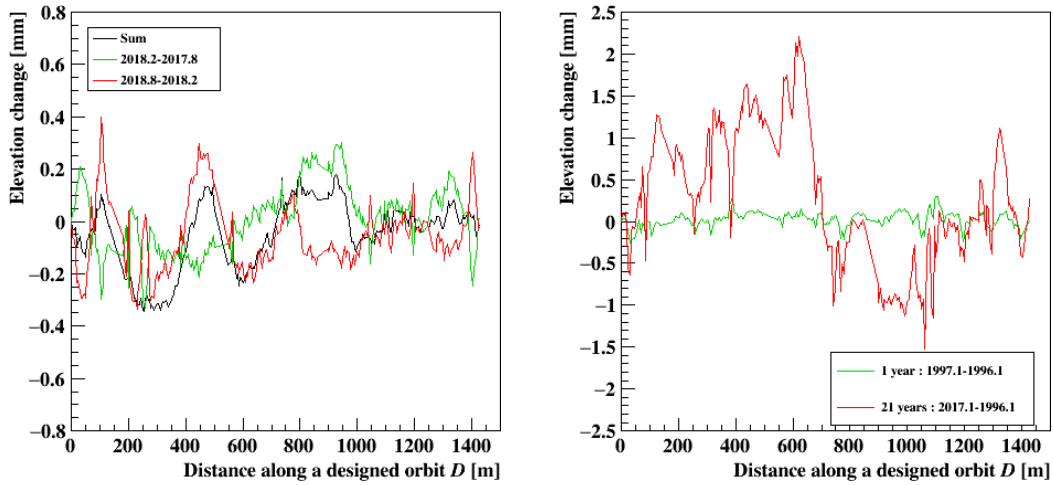

Figure 7. *Left*: seasonal elevation changes of storage ring magnets. *Dashed* and *dash-dot-lines* are elevation changes of 2018.8–2018.2 and 2018.2–2017.8 data sets, respectively. *Solid-lines* are their sum. *Right*: a comparison of 1 year (1997.1–1996.1, *dashed-line*) and 21 years (2017.1–1996.1, *solid-line*) changes of ground elevation around storage ring.

4 Interpretation of ground elevation by empirical *ATL*-law approach

The ground elevation changes of the SPring-8 storage ring are interpreted from the aspect of the empirical *ATL*-law in this section. As discussed above, we have over 20 years of rich survey data
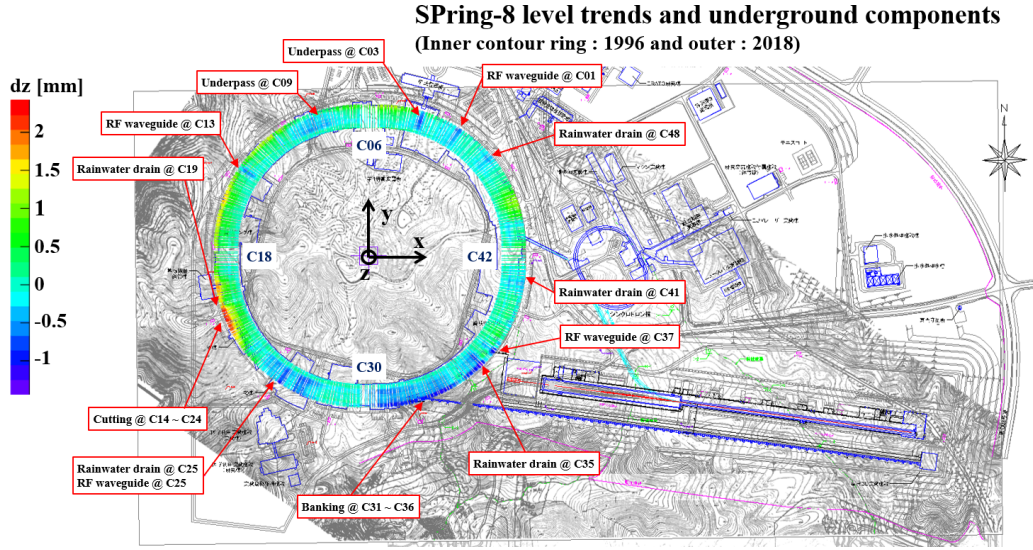
Figure 8. Measured SPring-8 accelerator component levels since 1996 overlaid on ground contour line map and infrastructures. Radial direction of contour ring represents elapsed years, i.e., inner of ring starts from 1996 and its outer ends in 2018. Typical length of one normal cell is ∼30 m.

sets for the SPring-8 storage ring magnets and found that $-1.5 \sim 2.5$ mm of ground elevation changes exist for these two decades.
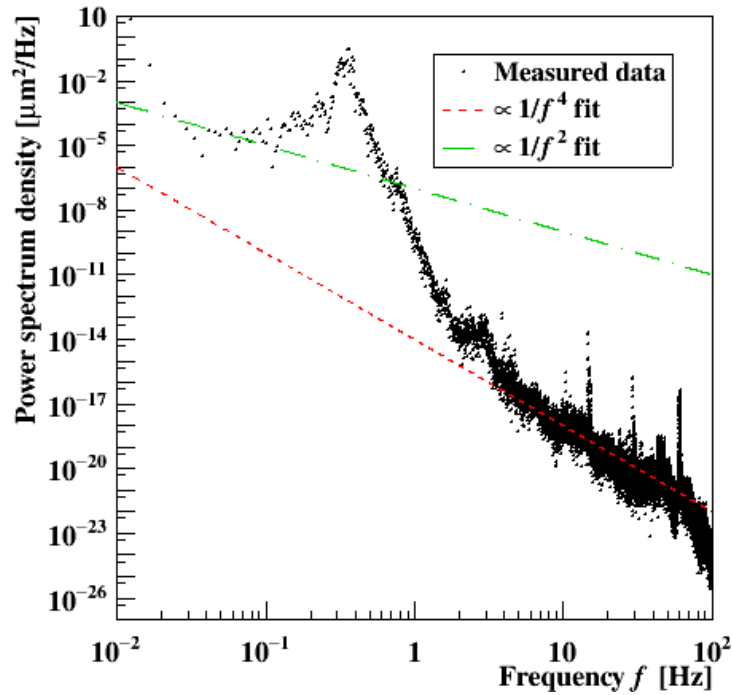

Figure 9. Power spectrum density (*dot*) of absolute ground motion measured at the SPring-8 storage ring on July 2003 overlaid with frequency dependent functions of $\propto 1/f^2$ (*dash-dot-line*) and $\propto 1/f^4$ (*dashed-line*). Data were measured during a scheduled power outage period.

Stochastic diffusive motion is investigated in geophysics because it is one candidate to provide ground motion among various well-known natural factors, including earth tides, activities of geologic faults, and periodic temperature and pressure changes that are reflected by both day-night and seasonal changes.

Figure 9 shows a power density spectrum of the ground motion measured in the SPring-8 accelerator tunnel on June 2003 by a Streckheisen STS-2 seismometer. Note that the measurement was done during a period in which the accelerator was not being operated. This spectrum indicates two major components: a peak around $0.1 \sim 1$ Hz and a noise structure over 1 Hz. The former structure is an effect of ocean waves, and the latter is cultural noises. The effects of earth tides generally appear around $10^{-5} \sim 10^{-4}$ Hz as peak structures. The power density spectrum of the ground motion decreased as $\propto 1/f^2$ for the lower frequency region ($f <\sim 0.1$ Hz), and thereafter, $\propto 1/f^4$ for the higher region ($f >\sim 0.1$ Hz) as frequency increased (figure 9). Massive ground motion associated with such earth tides is mostly transferred as elastic deformation or waves. The remaining part of the energy is consumed as plastic deformations and transferred as stochastic, i.e., Brownian or "random-walk" ground motions with a higher frequency [11].

The amplitude of the stochastic component is much smaller than the other components. Thus, it is generally discussed for such relatively stable environments as deep underground.
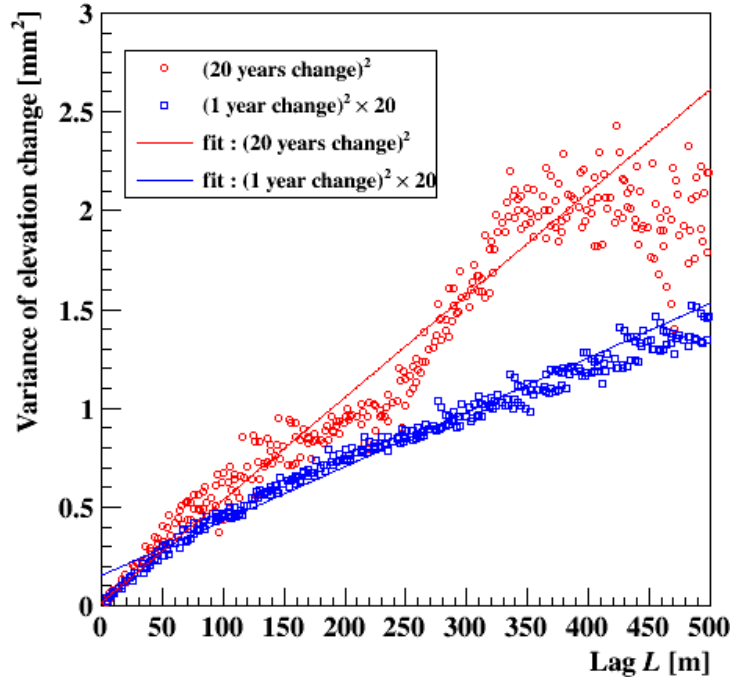

Figure 10. Variances of SPring-8 ground elevation changes over 1-year time intervals (multiplied by 20, *rectangle*) and 20 years (*circle*), correlated with lag L. *Solid-lines* for both plots are fitting examples with one-order linear functions.

In accelerator physics, Baklakov et al. [12] first proposed the ATL-law to describe the variance of ground elevation difference $\langle dz^2 \rangle$ between two points separated by distance L [m] over time interval T [years]:

$$\langle dz^2 \rangle \approx AT^{\alpha}L^{\beta}. \tag{4.1}$$

A is a coefficient that depends on the characteristics of the earth's crust. L is the distance along a designed electron beam orbit, not a straight line. Both $\alpha \approx 1$ and $\beta \approx 1$ in eq. (4.1) have been examined. Shiltsev scrutinized coefficient A for various accelerator facilities that were constructed underground except for SPring-8 [5].

Although SPring-8 was constructed above ground, this facility was built on relatively harder base rock than other storage ring facilities. Therefore, we applied the ATL-law to the variance of the elevation changes, assuming that the effects of day and night or seasonal temperature changes are averaged and canceled. Elevation change $dz(s)$ in time interval T ($T = 1, \cdots, 20$ years) at designed beam orbit coordinate s [m] is described:

$$dz(T, s) = z(t + T, s) - z(t, z),\tag{4.2}$$

where t demonstrated the survey year. Now, the variance of the ground elevation changes for a lag, i.e., the distance between arbitrary two surveyed points L and time interval T can be expressed:

$$\langle dz^2(T, L) \rangle = \frac{1}{M} \sum_M \frac{1}{N} \sum_N \{ dz(T, s + L) - dz(T, s) \}^2.\tag{4.3}$$

M and N are the number of pairs of time interval T and surveyed points distanced by L, respectively. Figure 10 shows the variances of the elevation changes that depend on the lag: $0 < L$ [m] < 500, which compare changes of 1 year (scaled multiplied by 20) and 20 years, i.e., $(T, M) = (1, 10), (20, 3)$ in eq. (4.3), respectively. The gradient is not unique, especially for a 20-year change.

We consider that the gradient change is systematic, i.e., not random. One candidate is the continuous lift up at the ground cutting area, which is distributed from C14 to C24 ($\sim$300 m long) and C31 to C36 ($\sim$150 m long), respectively as shown in figure 8. Such sources of systematic changes must be excluded from analysis data sets. However the amount of the data that correspond to the above condition is not negligible and further investigations are required to formulate installation and survey strategy and to discuss a necessity of realignment for the SPring-8 upgrade.

The gradients of the variance of the elevation changes for each time interval are evaluated with errors from eq. (4.3) depending on the lag and plotted in figure 11.

The coefficient in the empirical ATL-law that characterizes the earth's crust for the SPring-8 storage ring is eventually estimated as $A = (7.6 \pm 1.4) \times 10^{-6}$ μm^2/s/m. On the other hand, ground diffusion coefficients A for various accelerator facilities were already reported [5] (except those of SPring-8) and vary within $(0.2 \sim 40) \times 10^{-6}$ μm^2/s/m. Even though the SPring-8 storage ring is constructed on the ground level, its evaluated diffusion coefficient A is equivalent to ones of other accelerator facilities in deep underground. Thus SPring-8's ground itself can be estimated to be comparably firm.

5 Summary

The coordinates of the SPring-8 accelerator components were continuously surveyed and analyzed from 1996 to 2018. We compared and discussed seasonal and two decades of long-term trends for both horizontal and vertical coordinate changes of the accelerator components. For seasonal changes, the fluctuation of the radial direction change is twice as large as the azimuth one. The sum
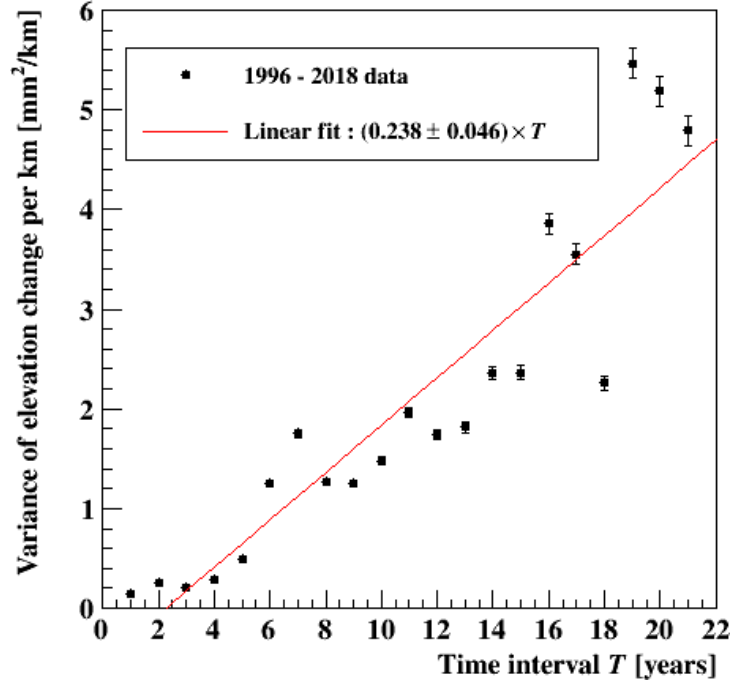
Figure 11. Correlations between variances of SPring-8 ground elevation changes per unit distance and survey time intervals.

of the two seasonal radial changes did not vanish and seems to be stored based on its long-term trend. Almost the same trend can be recognized for the elevation changes that are strongly affected by the original altitude distribution and such underground structures as RF waveguides, underpasses, and underground pipes.

The ground motion was analyzed and interpreted with the empirical ATL-law using two decades of elevation change data sets. The ground diffusion coefficient of $A = (7.6 \pm 1.4) \times 10^{-6}$ $\mu m^2/s/m$ was evaluated, and this result is found to be comparable to other data that were measured at various accelerator facilities. Further investigations, such as more precise identification of sources of relatively large systematic changes for the ground motion, are required for the future optimization and realignment of the SPring-8 storage ring.

References

[1] T. Suwada et al., *Real-time observation of dynamic floor motion of the KEKB injector linac with a laser-based alignment system*, *Phys. Rev. ST Accel. Beams* **20** (2017) 033501.

[2] C. Zhang, M. Hasegawa, K. Kanda and T. Shinomoto, *Performance of the iris diaphragm laser alignment system of the SPring-8*, in the proceedings of the 13th *International Workshop on Accelerator Alignment (IWAA2014)*, October 13–17 Beijing, China (2014).

[3] K. Fukami et al., *Performance verification of a precise vibrating-wire magnet alignment technique for next-generation light sources*, *Rev. Sci. Instrum.* **90** (2019) 054703.

[4] B.A. Baklakov et al., *Investigation of seismic vibration and relative displacements of linear collider VLEPP elements*, in the proceedings of the *1991 IEEE Particle Accelerator Conference (APS Beam Physics)*, May 6–9, San Francisco, U.S.A. (1991).

[5] V.D. Shiltsev, *Observations of random walk of the ground in space and time*, *Phys. Rev. Lett.* **104** (2010) 238501.

[6] R. Chasman and G. K. Green, *Design of a national dedicated synchrotron radiation facility*, OSTI 7334216 (1976).

[7] C. Zhang and S. Matsui, *Long-term variation of the magnet alignment in SPring-8 storage ring*, in the proceedings of the 11th *International Workshop on Accelerator Alignment (IWAA2010)*, September 13–17, Hamburg, Germany (2010).

[8] J.M. Calkins, *Quantifying coordinate uncertainty fields in coupled spatial measurement systems*, Ph.D. dissertation, Faculty of the Virginia Polytechnic Institute and State University, U.S.A. (2002).

[9] T.J.M. Kennie and G. Petie, *Engineering Surveying Technology*, Taylor & Francis, Oxfordshire U.K. (1990).

[10] T. Suwada, *Spatiotemporal diffusive evolution and fractal structure of ground motion*, *J. Phys. Soc. Jpn.* **87** (2018) 024901.

[11] M. Yoshioka, *Accelerator science and its civil and utility engineering work*, *J. Part. Accel. Soc. Jpn.* **3** (2006) 273.

[12] B.A. Baklakov et al., *Study of seismic vibrations for the VLEPP linear collider*, *Sov. Zh. Tech. Fiz.* **63** (1993) 123 [*Tech. Phys.* **38** (1993) 894].